Interfacial Microstructure and Intermetallics Developed in the Interface between In Solders and Au/Ni/Ti Thin Films during Reflow Process

KEESAM SHIN,[1] WON-GU CHO,[2] and YOUNG-HO KIM[2,3]

1.—Department of Metallurgy and Materials Science, Changwon National University, Kyungnam, 641-773, Korea, 2.—Department of Materials Engineering, Hanyang University, Seoul, 133-791, Korea. 3.—E-mail: kimyh@hanyang.ac.kr

Intermetallic phases and microstructures formed between In solder and Au/Ni/Ti thin films during reflow were characterized using x-ray diffraction (XRD), scanning electron microscopy (SEM), and transmission electron microscopy (TEM). Two types of two-step heat treatment were performed in a rapid thermal annealing (RTA) system or in a furnace to simulate the flip-chip solder-joining process. The $AuIn_2$ and $In_{27}Ni_{10}$ intermetallic phases were observed after the two-step heat treatment at the lower temperature. Additional In-Ni intermetallic layers formed between the $In_{27}Ni_{10}$ and Ni layer, which was two-step heat treated at the higher temperature. This phase was identified as metastable InNi of CsCl type with a = ~3.1 Å by convergent-beam electron diffraction (CBED).

Key words: Intermetallic compounds, In solder, η-$In_{27}Ni_{10}$, CsCl-type InNi

INTRODUCTION

Phase evolution in flip-chip solder joining is of great concern because the reliability of the joints is greatly influenced by the microstructures and the phases formed on the interfaces. This is a study on the evolution of microstructures and intermetallic phase in the In solder/Ni interface during flip-chip bonding. Indium and indium-alloy solders, such as In-Bi, In-Pb, and In-Sn, are used for laser-diode and photo-diode devices as well as liquid-crystal display application.[1–3] The under-bump metallurgy (UBM), the metallic pad for placing solder bumps at the desired location during flip-chip bonding by the reflow process, is composed of multilayers of thin films: protection layer/wetting layer/adhesion layer.[4,5] The Cu and Ni are very commonly used for the wetting layer, which reacts with the solder to form the intermetallic phase.[2,4–8] In flip-chip solder joining, spherical-shaped solder bumps are formed on the UBM pads of a chip through the reflow process, solder bumps are aligned to the substrate, and solder joints between the chips and the substrates were made by another reflow process. Interfacial reaction and intermetallic phases formed during the two-step reflow process influence the joint reliability.

(Received September 10, 2002; accepted December 2, 2002)

There are many studies and reports on the interfacial reactions between In and Cu.[8,9] It is well known that intermetallic phases, such as $Cu_{11}In_9$, Cu_7In_3, and Cu_2In, form in the solder/liquid In interface. However, limited results are available on intermetallic phases formed by the reaction between In and Ni. An η-phase $In_{27}Ni_{10}$ intermetallic compound was observed at the interface between In solders and Ni thin films[10,11] and at the interface between Pb-In solders and AuNi/Ni-P substrates.[12] Recently, it was reported that the Ni_2In_3 intermetallic phase in addition to $In_{27}Ni_{10}$ was observed in the In-Sn alloy/Ni-Cu-P interface[13] and the In/Ni interface.[11,14] These findings were the result of x-ray diffraction (XRD) and scanning electron microscopy (SEM) analyses that have limited application to in-depth chemical and microstructural investigation of intermetallic phases. Very thin layers of other phases besides $Ni_{10}In_{27}$ and Ni_2In_3 phases could form that may not be detected by XRD or SEM analyses. Analyses using transmission electron microscopy (TEM) would be much more powerful for the purpose, but the TEM analyses have been limited so far by the complexity in the analyses and specimen preparation.

In this study, an XRD designed for thin-film characterization and a field-emission SEM (FESEM) were used for chemical and crystallographic char-

acterization of the interfacial microstructures and intermetallic compounds formed during the reflow process by the interdiffusion between liquid In solder and Au/Ni/Ti UBM. For more thorough analyses of the phases unidentified with the XRD and FESEM, TEM analyses were carried out applying such techniques as convergent-beam electron diffraction (CBED) and energy dispersive x-ray spectroscopy (EDS).

EXPERIMENTAL PROCEDURE

The 150-nm-thick Ti-adhesion layer, the 200-nm-thick Ni-wetting layer, and the 50-nm-thick Au-oxidation protection layer were sequentially deposited on the Si wafer using electron-beam evaporation. Then, the 1-μm-thick In solder was evaporated on the Au/Ni/Ti films from the resistance-heated source. Under the simulated conditions of the reflow process, the specimens were reflowed twice in a N_2 atmosphere using a rapid thermal annealing (RTA) system or a tube furnace. The melting point of In is 156.7°C, so the two rapid heat treatments were performed at the peak temperatures of 180°C and 185°C (designated as RTA180-RTA185), which were the simulated conditions of solder-bump formation and subsequent joining of the chip to the substrate. In addition, specimens were heat-treated at 250°C in an RTA system and at 255°C in a tube furnace (designated as RTA250-FT255) to investigate the effect of reflow temperature on the formation of intermetallic compounds.

The intermetallic compounds were analyzed using XRD equipped with a thin-film attachment at the experimental conditions of incident angles of 1–7°, and x-ray power of 4 kW with Cu $K\alpha_1$. The cross sections of RTA180-RTA185 and RTA250-FT255 specimens, cut and etched in a solution of HNO_3, HCl, and distilled water of 1:7:8 in volume ratio, were analyzed using FESEM. For cross-sectional observation and analyses of TEM specimens of RTA180-RTA185 and RTA250-FT255, two In/Au/Ni/Ti/Si specimens of the same condition were bonded vis-à-vis using epoxy with curing at room temperature, which were then diamond-sawed, supersonic-disc cut to 3 mm in diameter, and were subsequently ground to 100-μm thick. The specimens were then dimpled and ion milled to electron transparency. The cross-sectional TEM specimens were successfully prepared using an ion-milling technique known as the sector speed-control method, in which the rotational speed of the specimen during ion milling was drastically reduced to milling speed of the interface region from its normal running speed when the guns and the line of bonding were in angles between ±40°. The incident angle of the ion beam was ~11° to the horizontal specimen surface, with stage cooling with liquid nitrogen to extract the heat generated during ion milling and avoid specimen damage. The TEM analyses were carried out at an acceleration voltage of 200 kV.

RESULTS AND DISCUSSION

Analysis of the Intermetallic Compounds Using X-ray Diffraction

Figures 1 and 2 are the XRD θ-2θ scan and 2θ of thin-film analysis results of RTA180-RTA185 and RTA250-FT255, respectively. In thin-film XRD analysis, a beam of x-ray is delivered in a low angle to the specimen surface and collects diffracted x-rays, which are mostly generated from the specimen surface. The diffraction-pattern analysis results show that $AuIn_2$ and $In_{27}Ni_{10}$ (η phase) are formed at the interface of In and Ni. When the incident angle was 5° or lower, the thin-film XRD patterns of RTA180-RTA185 were identical and had the same results as those of θ-2θ analyses, indicating that $AuIn_2$ and $In_{27}Ni_{10}$ were formed. When the incident angle was 7°, the Ni (111) peak as well as those of In, $AuIn_2$, and $In_{27}Ni_{10}$ appeared, which indicated that the 200-nm-thick Ni film and In interacted, but the Ni was not exhausted by the reaction. The thin-film XRD patterns

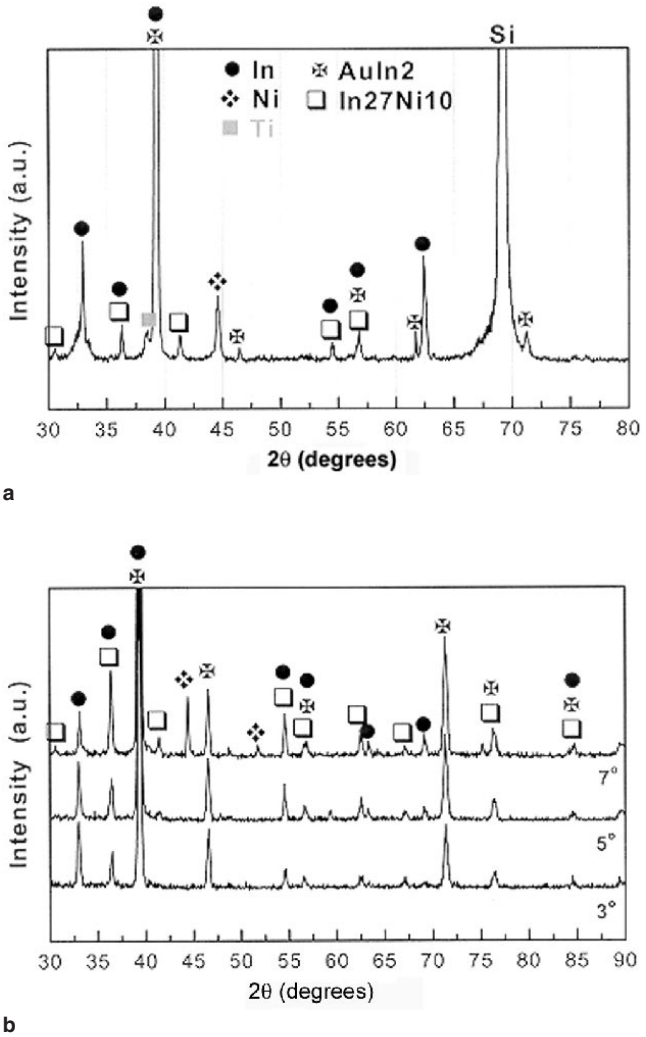

Fig. 1. The powder and thin-film XRD patterns obtained from the RTA 180-RTA185 sample.

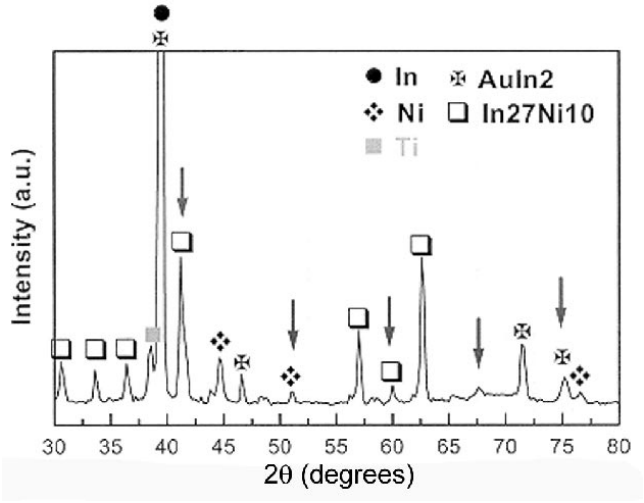

a

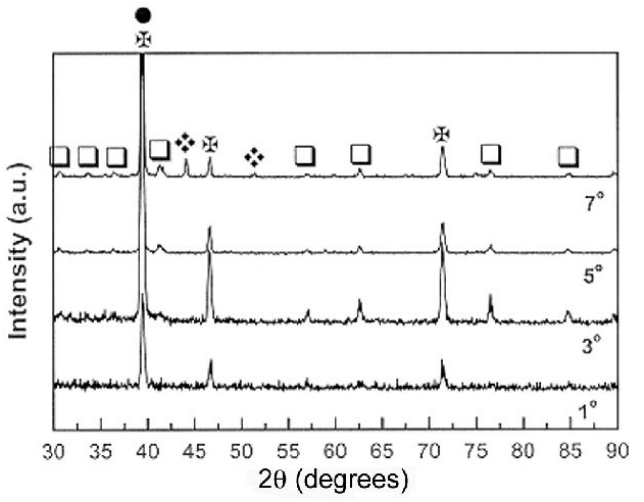

b

Fig. 2. The powder and thin-film XRD patterns obtained from the RTA250-FT255 sample.

of RTA250-FT255 showed that $AuIn_2$ and $In_{27}Ni_{10}$ formed at the interface between the In and Ni thin films, as was the case in RTA180-RTA185. Peaks of Ni and $In_{27}Ni_{10}$ also appeared when the incident angle of the thin-film x-ray analyses was increased to 3–7° from 1°, where only In and $AuIn_2$ peaks appeared. The XRD analyses indicated that intermetallic compounds of $AuIn_2$ and $In_{27}Ni_{10}$ were formed in the interfaces of In solders and Ni thin films in both specimens of RTA180-RTA185 and RTA250-FT255. As the angle of incidence gradually increased in the thin-film XRD analyses, the phases of the multilayers were sequentially identified, and the order was found to be $In/AuIn_2/In_{27}Ni_{10}/Ni$ from top to bottom.

When multiphase spectra are analyzed, there is a possibility of failing to identify a phase when peaks of the phase overlap with those of others. Although it is not obvious in the spectra of RTA250-FT255, the previous papers have reported the formation of In_3Ni_2 (δ phase, hexagonal) in addition

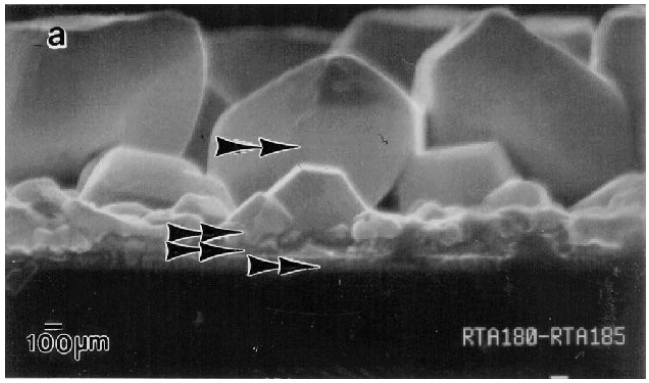

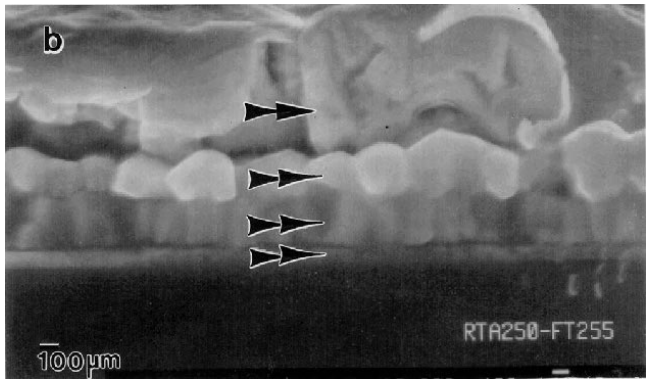

Fig. 3. The FESEM images obtained from (a) the RTA180-RTA185 cross-sectional sample and (b) the RTA250-FT255 cross-sectional sample.

to $In_{27}Ni_{10}$ (η phase, cubic).[11,13,14] However, those peaks could also be interpreted as those of $In_{27}Ni_{10}$, which is a good reason for TEM/SEM analyses of the specimens in addition of the microstructural characterization.

Microstructural Observation and Analysis of the Intermetallic Phases

Figure 3a and b are cross-sectional FESEM micrographs of RTA180-RTA185 and RTA250-FT255, respectively. From bottom to top, the micrographs show that RTA180-RTA185 consists of (1) the Si substrate, (2) three relatively nonuniform layers of ~100-nm thickness, and (3) a relatively uniform ~1-μm-thick, equiaxed intermetallic compound. The micrographs of RTA250-FT255 show four types of films on the Si substrate as shown in RTA180-FT185 with some difference in microstructures, i.e., (1) the Si substrate, (2) a relatively uniform layer of ~100-nm thick, (3) ~300-nm-thick film of columnar phase, (4) ~300-nm-thick film of equiaxed phase, and (5) ~1-μm-thick film of equiaxed phase. The FESEM analysis of the cross sections of both types of the specimens shows the four layers of films on top of the Si substrate, revealing no new phase compared to the results of the XRD analysis.

Figure 4a and b are TEM bright-field images of cross-sectional specimens of RTA180-RTA185, show-

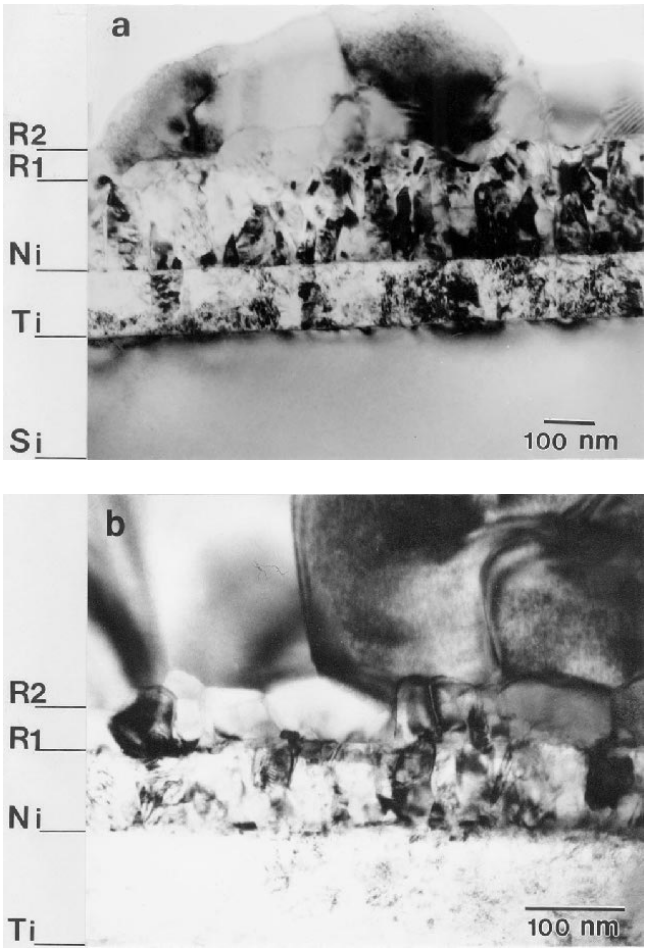

Fig. 4. The bright-field TEM images of the RTA 180-RTA185 cross-sectional sample.

ing there are four layers of films on the Si substrate as observed by FESEM. The two micrographs show four layers on top of the Si wafer, depending on the level of ion milling. The micrographs show that the two layers adjacent to the Si wafer were grown as columnar grains, on top of which formed ~70-nm-thick equiaxed grains (designated as the R1 layer) and another layer of large grains (designated as R2). The EDS analyses indicate that the two columnar layers adjacent to the Si wafer are of Ti and Ni, confirming the XRD results, which indicated the incomplete exhaustion of the 200-nm-thick Ni by the reaction during the two rapid heat treatments. The clear interface can be interpreted as an indication of no reaction between Ti and Ni in the given heat treatment. The ~100-nm-thick third layer and 1-μm-thick fourth layer of equiaxed grains observed on the Si substrate by FESEM are, thus, of R1 and R2, respectively.

Figure 5a and b are the respective CBED patterns from R1 and R2 layers. Using D_1, D_2, and CRAD, which are the respective distances from the transmitted beam of (000) to the two discs of nearest zeroth order Laue zone (ZOLZ) and higher order Laue zone (HOLZ) continuous discs in CBED patterns, the volume of the primitive cell can be calculated, which, in turn, can be used for the quick and reliable phase identification.[15] As shown in Eq. 1, a primitive-cell volume can be calculated by dividing the projected area by the reciprocal spacing.

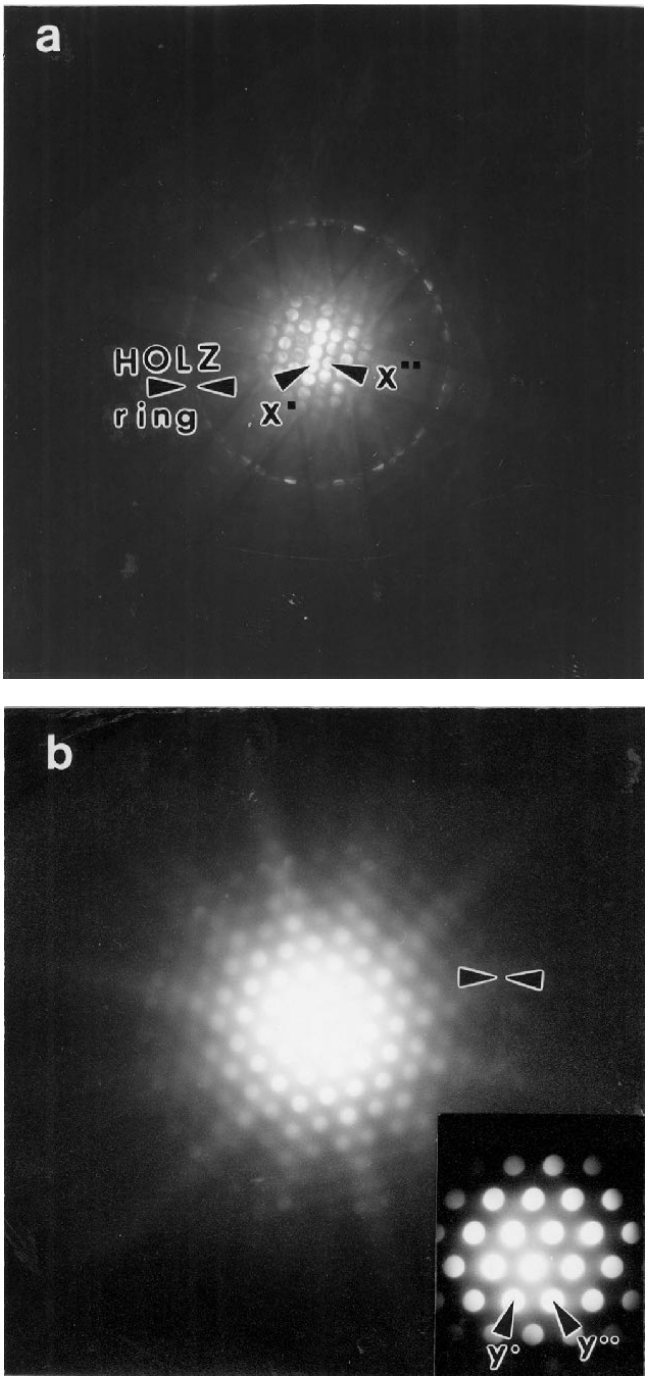

Fig. 5. The CBED patterns obtained from (a) the R1 layer and (b) the R2 layer of the RTA180-RTA185 cross-sectional sample.

$$\text{volume of the primitive cell} = \frac{CL^2\lambda^3}{D_1D_2 \sin(\text{ANG})\left[1.0 - \cos\left(\tan^{-1}\frac{\text{CRAD}}{\text{CL}}\right)\right]} \quad (1)$$

where CL is camera length; λ is wavelength of the electron beam, which is 0.02508 Å for 200 keV; and ANG is the angle between the two ZOLZ discs chosen such that it is not larger than 90°. The volumes of the primitive cells of major intermetallic compounds between In, Au, Ni, Ti, In-Ni, and In-Au are listed in Table I. The primitive-cell volume of the R1 layer was 415 $Å^3$, calculated using Eq. 1 with the values of D_1, D_2, CRAD, and ANG measured from Fig. 5a, the values of which are listed in Table II. The EDS analysis revealed that the R1 layer was composed of 76.1at.%In and 23.9at.%Ni on average. Based on the primitive-cell volume and chemical composition obtained from CBED and EDS examination, the R1 layer is believed to be $In_{27}Ni_{10}$ (η phase) of a theoretical unit-cell volume of 389 $Å^3$, and a chemical composition of 73at.%In and 27at.%Ni. The results of the ZOLZ ring-pattern analyses using a camera constant of 7.40 mm Å revealed that the rings of x′ and x″ are respective diffraction spots of (200) and (121). Figure 5b is the CBED pattern obtained with a camera length of 110 mm. Calculation with the measured data listed in Table II resulted in the primitive volume of 66 $Å^3$. The calculated volume of primitive cell and the EDS data of the composition of 66.7at.%In and 33.3at.%Au indicated that it was $AuIn_2$. Therefore, the spots of y′ and y″ are those of (220) and (202) planes, respectively. From the TEM results, it is understood that the columnar phases of 1-μm and ~70-nm thickness observed by FESEM are $AuIn_2$ and $In_{27}Ni_{10}$, respectively.

The TEM bright-field images of the cross section of RTA250-FT255 (Fig. 6) show details of the layers adjacent to the Si wafer (Fig. 6a and b), and equiaxed grains formed on top of the columnar grains (Fig. 6c). It is understood from the observation that, from the Si wafer upward, three layers of films thinner than 150 nm, columnar grains of ~55-nm thick (denominated as F2), and large equiaxed grains (denominated as F3) were formed. The films were analyzed using CBED and EDS as

Table I. Primitive-Cell Volume of the Possible Intermetallic Compounds among In, Au, Ni, and Ti

Phase	Primitive-Cell Volume Crystal Structure	Phase	Primitive-Cell Volume Crystal Structure
In	26.15 $Å^3$ Tetragonal, I4/mmm, V52.30 $Å^3$	$Au_{11}In_3$	247.90 $Å^3$ Orthorhombic, Cm2m, V495.79 $Å^3$
Au	16.96 $Å^3$ Cubic, Fm3m, V67.85 $Å^3$	$Au_{10}In_3$	460.36 $Å^3$ Hexagonal, P$\bar{3}$, V460.36 $Å^3$
Ni	10.94 $Å^3$ Cubic, Fm3m, V43.76 $Å^3$	Au_3In	139.19 $Å^3$ Hexagonal, P63/mmc, V139.19 $Å^3$
Ti	35.32 $Å^3$ Hexagonal, P63/mmc, V35.32 $Å^3$	Au_9In_4	949.57 $Å^3$ Cubic, P$\bar{4}$33m, V949.57 $Å^3$
$In_{27}Ni_{10}$ (η phase)	388.84 $Å^3$ Cubic, Im3m, V777.67 $Å^3$	Au_7In_3	1,099.50 $Å^3$ Hexagonal, P$\bar{3}$, V1099.50 $Å^3$
In_3Ni_2 (δ phase)	88.73 $Å^3$ Hexagonal, P$\bar{3}$ml, 88.73 $Å^3$	Au_3In_2	163.33 $Å^3$ Hexagonal, P3ml, V163.33 $Å^3$
InNi (ε phase)	103.57 $Å^3$ Hexagonal, P6/mmm, V103.57 $Å^3$	Au_4In	35.18 $Å^3$ Hexagonal, P63/mmc, V35.18 $Å^3$
$InNi_2$	77.89 $Å^3$ Hexagonal, p63/mmc, V77.89 $Å^3$	$AuIn_2$	69.20 $Å^3$ Cubic, Fm3m, V276.79 $Å^3$
$InNi_3$	77.26 $Å^3$ Hexagonal, P63/mmc, V77.26 $Å^3$	$InNi_3$ (γ phase)	104.63 $Å^3$ Hexagonal, P63/mmc, V104.63 $Å^3$

Table II. The CBED and EDS Results of the Formed Intermetallic Compounds (λ = 0.0251 Å)

Sample	Layer	D1 (mm)	D1 (mm)	ANG (°)	CRAD (mm)	CL (mm)	Primitive Cell Volume ($Å^3$)	EDS Result (at.%) (Identified Phase)
RTA 180–RTA 185	R1	1.61	1.94	65	14.75	300	415	76.1In-23.9Ni ($In_{27}Ni_{10}$)
	R2	1.20	1.20	60	7.50	110	66	64.3In-35.7Au ($AuIn_2$)
RTA 250–FT 255	F1	2.40	5.40	90	26.00	300	29	50.6–61.8In-49.4–38.2Ni (InNi)
	F2	1.14	1.95	74.5	17.30	300	400	72.3In-27.2Ni ($In_{27}Ni_{10}$)
	F3	2.00	5.05	83	19.30	300	69	64.2In-35.8Au ($AuIn_2$)

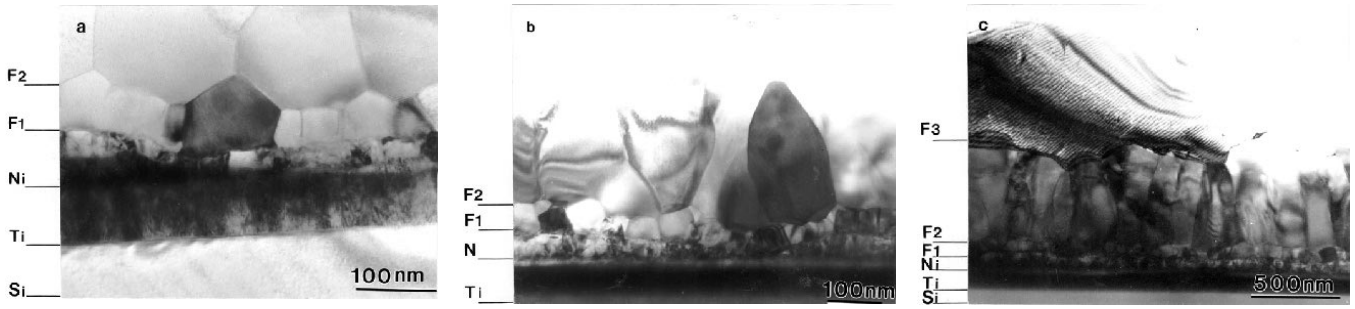

Fig. 6. The bright-field TEM images of the RTA250-FT255 cross-sectional sample.

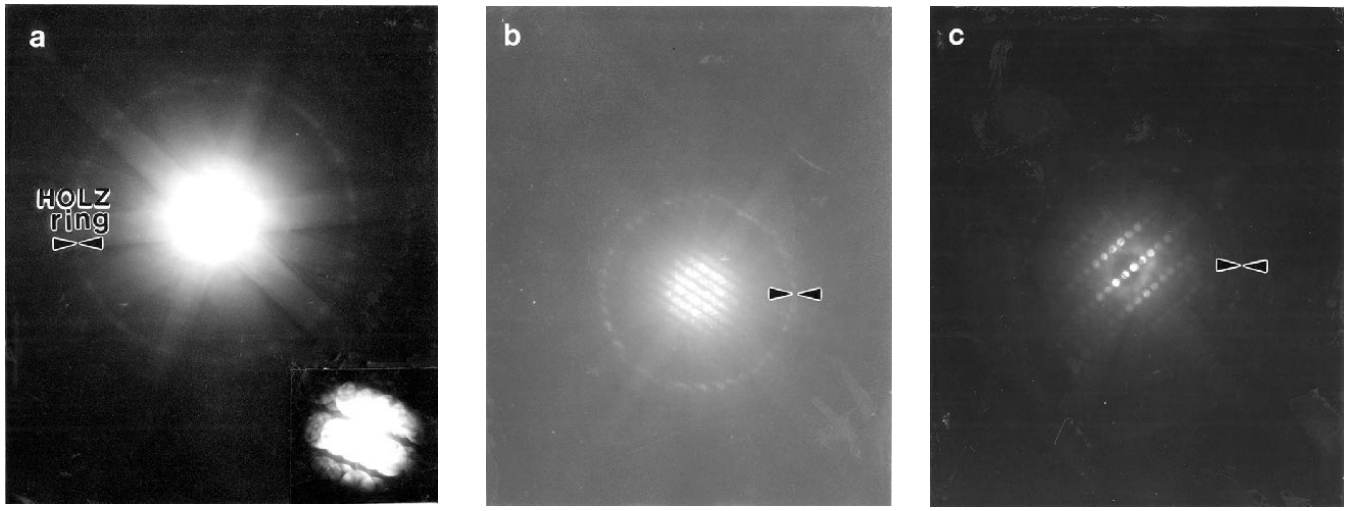

Fig. 7. The CBED patterns obtained from (a) the F1 layer, (b) the F2 layer, and (c) the F3 layer of the RTA250-FT255 cross-sectional sample.

were analyzed the RTA180-RTA185 specimen. The results of EDS revealed that the two layers adjacent to the Si wafer were of Ti and Ni. Figure 7a–c is the respective CBED patterns of the columnar grains (denominated as F1) on top of the Ni thin film, of F2 and of F3 layers recorded at a camera length of 300 mm and acceleration voltage of 200 keV. Using the measured data (listed in Table II) of D_1, D_2, CRAD, and ANG from Fig. 7a, the primitive-cell volume was calculated as 29 Å^3. The EDS analysis showed that the F1 layer is composed of 50.6at.%In and 49.4at.%Ni in average. Because the F1 layer is thinner than 150 nm, a smaller probe is desired for better spatial resolution, which may lower the statistical reliability of the EDS quantitative data because of the reduced intensity of the x-ray signal. Based on results of XRD analyses by Lee et al.[11] and by Tseng et al.,[14] the F1 layer was anticipated to be In_3Ni_2 (δ phase, hexagonal, $P\bar{3}$ m1). However, the volume of 29 Å^3 determined using CBED analysis (Table II) was not in agreement with the actual value of 89 Å^3. Figure 8 is the microdiffraction pattern of the F1 layer; the analysis of which indicated that it was not of In_3Ni_2. As shown in Table I, there is no In-Ni binary phase whose primitive-cell volume is 29 Å^3; thus, it is believed that the F1 layer is the metastable phase formed during heat treatment of In solder and Ni

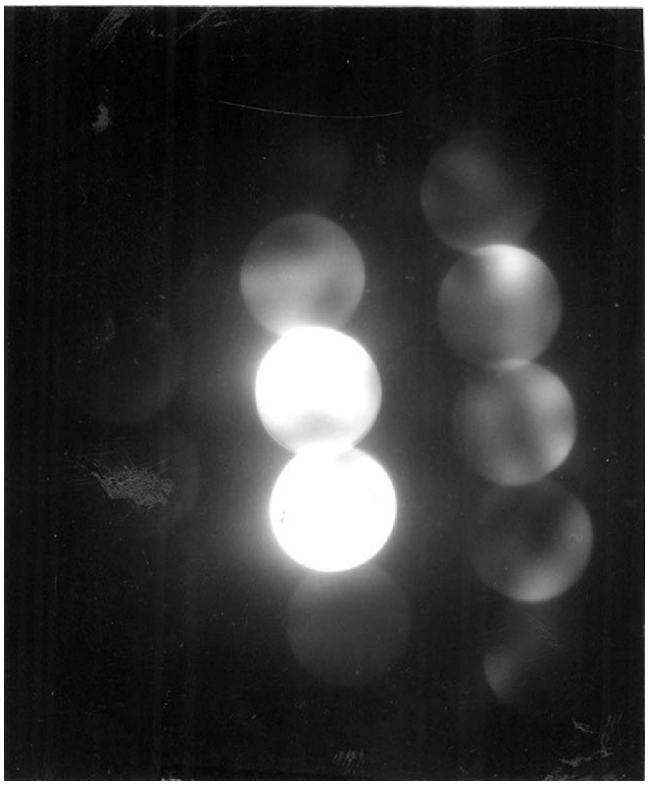

Fig. 8. The microdiffraction pattern obtained from the F1 layer.

film, or stable but not known. To determine the phase of the In-Ni of layer F1, CBED patterns of different zone axes and microdiffraction patterns were analyzed (Fig. 9) and earned 29–32 Å^3 for primitive-cell volume. Metastable d-InNi phase, which has a CsCl structure, was reported.[16] With a clue from the small primitive-cell volume and EDS results, the CsCl structure was assumed, and the patterns of Figs. 7a, 8, and 9a and b were successfully identified as zone axes patterns of [0$\bar{2}$1], [1$\bar{1}\bar{3}$], [1$\bar{2}\bar{1}$], and [$\bar{1}\bar{5}$3]. Those results are in agreement with the selected-area diffraction patterns shown in Fig. 10, which are zone axes patterns of [001] and [122], respectively. In Table III, 2θ and structure factors of each diffracting planes are listed assuming the lattice parameter of ~3.1 Å. The arrows

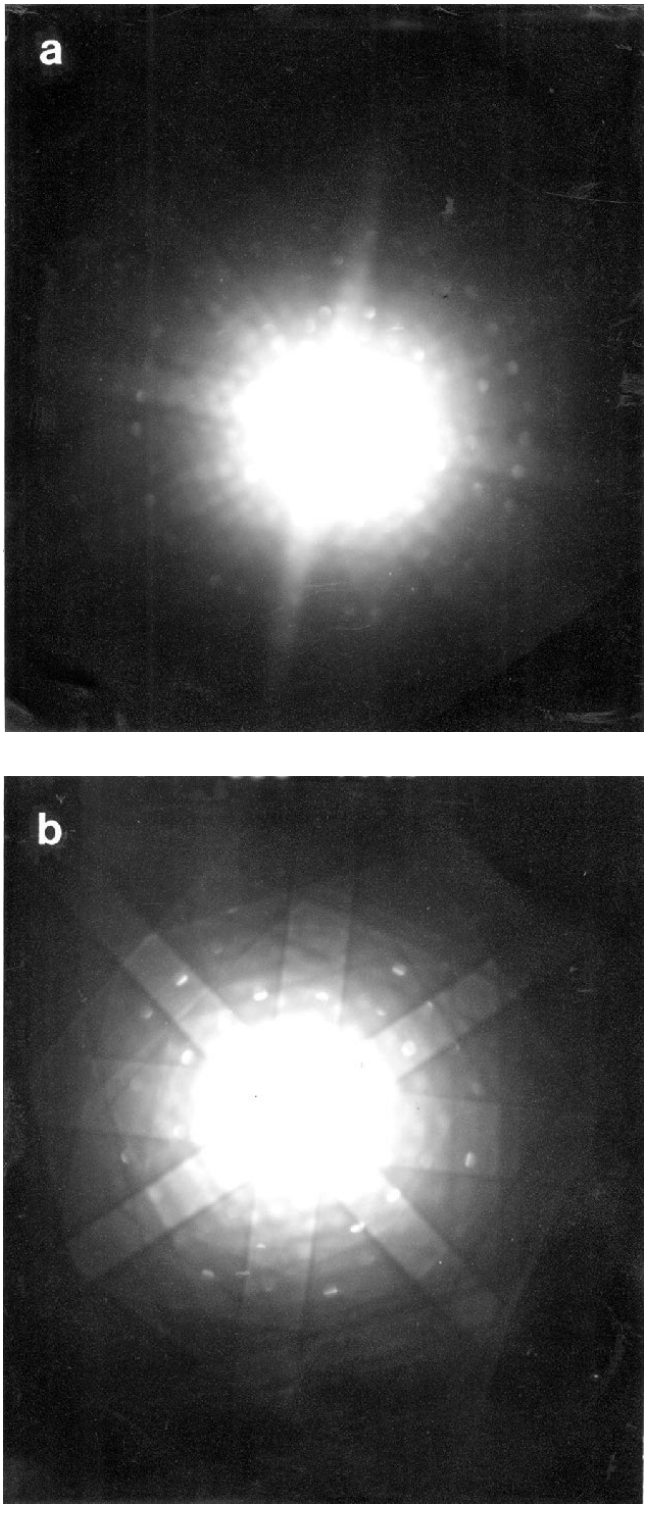

Fig. 9. The CBED patterns obtained from the F1 layer at two different zone axes: (a) [1$\bar{2}\bar{1}$] and (b) [$\bar{1}\bar{5}$3].

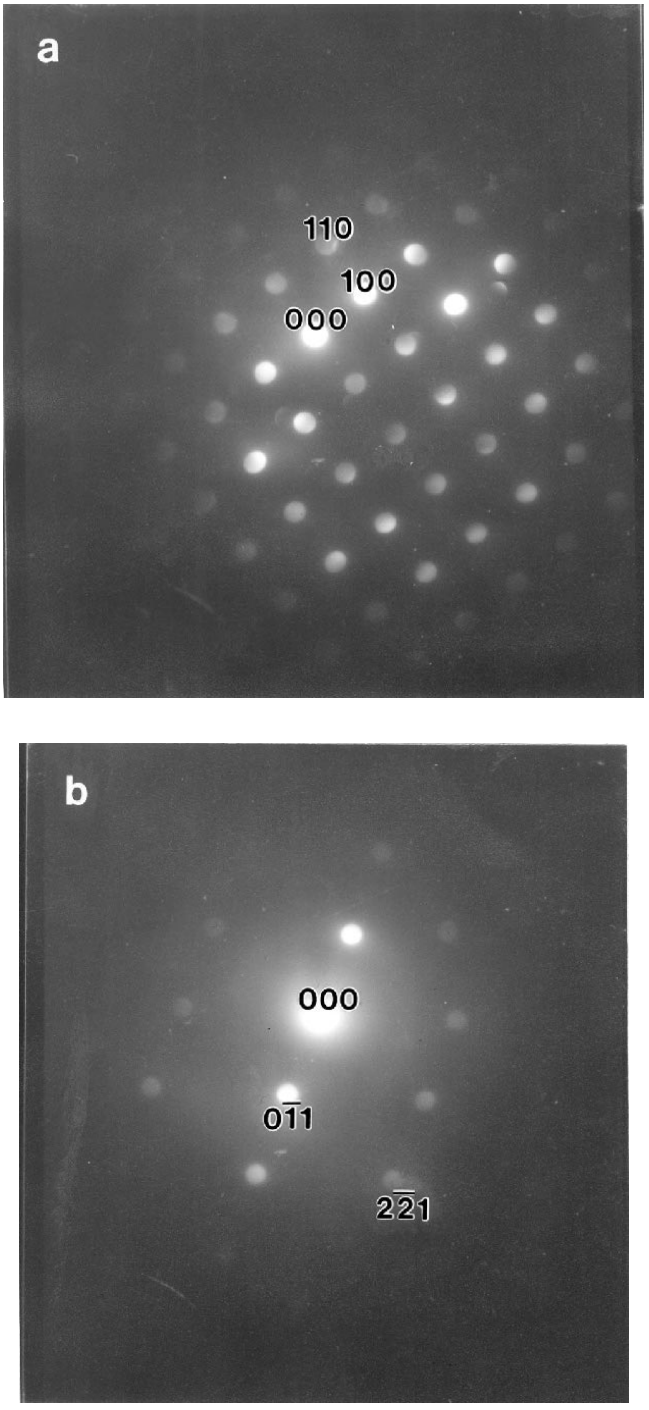

Fig. 10. The selected-area diffraction patterns at two zone axes: (a) [001] and (b) [122].

Table III. XRD Analysis Data for Simple Cubic Structural InNi

hkl	Diffraction Angle (2θ)	Structure Factor, F
100	28.80°	$f_{In} - f_{Ni}$
110	41.08°	$f_{In} + f_{Ni}$
111	51.03°	$f_{In} - f_{Ni}$
200	59.65°	$f_{In} + f_{Ni}$
210	67.56°	$f_{In} - f_{Ni}$
211	75.05°	$f_{In} + f_{Ni}$

in Fig. 2 indicate the positions of the InNi peaks of the RT250-FT255 specimen; most of which overlap with peaks of other phases. Chen and Lin observed the cubically shaped intermetallic crystals, which were identified as In_3Ni_2 and $In_{27}Ni_{10}$ by XRD analysis.[13] The morphology of intermetallic crystals indicates that those cubically shaped intermetallic crystals are likely to be nonequilibrium InNi and $In_{27}Ni_{10}$ that have a cubic structure.

With D_1, D_2, and ANG measured from the CBED pattern of F2 (Fig. 7b), the primitive-cell volume of the F2 layer was calculated as 400 Å^3. In addition, EDS analysis showed that F2 is composed of 72.3at.%In and 27.7at.%Ni. Therefore, the F2 layer is believed to be $In_{27}Ni_{10}$. The diffraction pattern of Fig. 7c and EDS results indicate that the In solder and Au reacted to form the columnar grains of $AuIn_2$. Based on the earlier observation using XRD and FESEM, it is believed that the F3 layer, the columnar grains of 1 μm, is of $AuIn_2$ phase. Thus, the two layers of 300-nm thick are believed to be $In_{27}Ni_{10}$ and InNi, respectively. As shown in Fig. 6a and b, the irregular thickness of the Ni film is believed to be the result of incomplete exhaustion of Ni during the reaction in the reflow process.

SUMMARY AND CONCLUSIONS

In this study, ~1-μm-thick indium film was deposited on the UBM film of Au (~50 nm)/Ni (~200 nm)/Ti (~150 nm) on a Si substrate, and the intermetallic compound formation during reflow process was examined. The In solder on Au/Ni/Ti was heat treated at two different two-step heat-treatment conditions (RTA180-RTA185 and RTA20-FT255), which were then examined with XRD, SEM, and TEM for microstructural and phase analyses. The TEM CBED analysis was successfully applied to identify a phase, which could not be analyzed otherwise. The followings are conclusions from the study.

- The XRD analyses revealed that the RTA180-RTA185 consisted of films of In/$AuIn_2$/$In_{27}Ni_{10}$/Ni from the top of the Si wafer substrate. The XRD analyses for RTA250-FT255 showed the same result as that of RTA180-RTA185, which were confirmed by SEM/EDS analyses.
- The TEM bright-field observation of the cross section of the specimens and CBED analyses revealed that there is an InNi phase formed between the Ni layer and $In_{27}Ni_{10}$ in the RTA250-FT255 specimen.
- The metastable InNi is found to be a CsCl-type cubic structure with a lattice parameter of ~3.1 Å.
- Table IV summarizes the results of the combined microstructural analyses.

ACKNOWLEDGEMENTS

The work was supported by Center for Electronic Packaging Materials of Korea Science and Engineering Foundation.

REFERENCES

1. J.T. Moon, S.H. Lee, K.J. Joo, H.T. Lee, M.G. Song, and K.A. Pyun, *Kor. J. Mater. Res.* 7, 330 (1997).
2. M. Mori, Y. Kizaki, M. Saito, and A. Hongu, *IEEE Trans. Comp., Hydrids, Manuf. Technol*. 16, 852 (1993).

Table IV. Microstructures and Phases Identified to Form at the Interfaces between the In Solder and Au/Ni/Ti UBM

Initial Coating	Microstructure after Heat Treatment	Sequence of Phases
(a) RTA180-RTA185		
5) In: ~1 μm	R2: t = ~1 μm: equiaxed grains	$AuIn_2$
4) Au: 50 nm	R1: t = ~100 nm: equiaxed grains	$In_{27}Ni_{10}$
3) Ni: 200 nm	t = ~100 nm: columnar: Ni (not exhausted)	Ni
2) Ti: 50 nm	t = ~100 nm: columnar, uniform thickness	Ti
1) Si: wafer	Si wafer	Si wafer
(b) RTA250-FT255		
—	F3: large equiaxed grains	$AuIn_2$
5) In: ~1 μm	F2: t = ~550 nm: columnar	$In_{27}Ni_{10}$
4) Au: 50 nm	F1: t ≥ 150 nm: equiaxed	InNi
3) Ni: 200 nm	Ni, t ≥ 150 nm: columnar	Ni
2) Ti: 50 nm	Ti, t ≥ 150 nm: uniform thickness	Ti
1) Si: wafer	Si wafer	Si wafer

3. J.C. Hwang , *IEEE Trans. Comp. Packag. Manuf. Technol. Part A* 18, 458 (1995).
4. J.H. Lau, *Flip Chip Technologies* (New York: McGraw-Hill, 1996), pp. 123–126.
5. R.R. Tummala, E.J. Rymaszewski, and A.G. Klopfenstein, *Microelectronics Packaging Handbook Part II* (New York: Chapman & Hall, 1997), pp. 129–185.
6. E.K. Yung and I. Turlik, *10th IEPS Conf. Proc.* 1065 (1990).
7. K. Mizuishi and T. Mori, *IEEE Trans. Comp., Hybrids, Manuf. Technol.* 11, 481 (1988).
8. K.P. Gurov, V.N. Pimenov, and S.G. Radkovskiy, *Russ. Metall.* 3, 52 (1978).
9. C.R. Kao, *Mater. Sci. Eng.* A238, 200 (1997).
10. R. Davenaux and I. Turlik, *IEEE Trans. Comp., Hydrids, Manuf. Technol.* 13, 929 (1990).
11. C.-Y. Lee, Y.-H. Kim, and C.S. Kim, *J. Kor. Inst. Metal Mater.* 35, 1395 (1997).
12. K.T. Puttlitz, , *IEEE Trans. Comp., Hydrids, Manuf. Technol.* 13, 647 (1990).
13. C.J. Chen and K.L. Lin, *IEEE Trans. Comp. Packag. Manuf. Technol. Part B* 20, 211 (1997).
14. Y.H. Tseng, M.S. Yeh, and T.H. Chuang, *J. Electron. Mater.* 28, 105 (1999).
15. G.H. Kim, *Bull. Kor. Inst. Metal Mater.* 9, 633 (1996).
16. T.B. Massalski, *Binary Alloy Phase Diagrams,* vol. 2 (Metals Park, OH: ASM, 1986), p. 1386.